SYMMETRIC NIP
MECHANICS

By

DEVASHISH MUNSHI

Master of Science
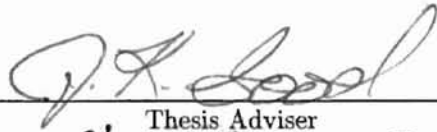
Oklahoma State University
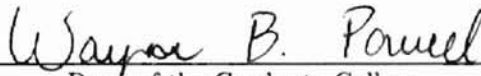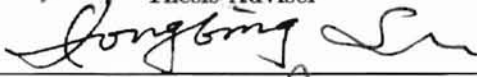
Stillwater, Oklahoma

1999

Submitted to the Faculty of the
Graduate College of the
Oklahoma State University
in partial fulfillment of
the requirements for
the Degree of
MASTER OF SCIENCE
May, 1999

SYMMETRIC NIP
MECHANICS

Thesis Approved:

_____
Thesis Adviser

_____

_____

_____
Dean of the Graduate College

ACKNOWLEDGEMENTS

TABLE OF CONTENTS

LIST OF FIGURES

NOMENCLATURE

A_n, B_n Fourier Coefficients, equations 3.9, 3.10, 3.11

E Young's modulus

h_m Fourier coefficients, equation 3.15

$\tilde{h}_m$ Fourier coefficients, equation 3.16

L_0 total length of contact nip divided by 2

$M, \bar{M}$ maximum number of terms

r radial coordinate

$\bar{r}$ r/R_0

R_0 outer radius of cylinder

R_i radius of hard core

$\bar{R}_i$ R_i/R_0

s nip coordinate, measured from $\theta = 0$

$(tE)_p$ extensional stiffness of the sheet

U Stress Function

u radial displacement

$\bar{u}$ u/R_0

u_0 maximum indentation (a negative quantity)

v tangential displacement

$\bar{v}$ v/R_0

$V_{(1)}, V_{(2)}$ peripheral speed of cylinders (1) and (2)

$\alpha_n, \bar{\alpha}_n$ equation 3.19

$\beta_n, \bar{\beta}_n$ equation 3.23

δ displacement of roller center

ϵ_p strain in the sheet

ϵ_θ tangential strain in the elastic layer of the cylinders

κ, β material constants related to Poisson's ratio

ν Poisson's ratio

Ω one half of the total contact angle

θ angular coordinate

σ_r radial stress

$\bar{\sigma}_r$	σ_r/E
σ_θ	tangential stress
$\bar{\sigma}_\theta$	σ_θ/E
$\tau_{r\theta}$	shear stress
$\bar{\tau}_{r\theta}$	$\tau_{r\theta}/E$
μ_{rr}	coefficient of friction between elastic layers
μ_{rp}	coefficient of friction between elastic layer and the sheet

Note: Any departure from these notations in an equation has been explicitly mentioned.

CHAPTER 1

INTRODUCTION

A web is a thin continuous flexible material. Common web materials are newsprint, magnetic tape, and photographic film. Many packaging materials, for example polypropylene and polyethylene, come in web form. Web materials are usually stored in the form of rolls.

There are many situations where a web material is driven through two impinging rubber covered rollers, notable examples are printers, photocopy machines and tape drives. Two cases can be considered. First, the web has no net traction, which is the symmetric case. And second, the web in the nip is being pulled or pushed by a tangential force while it is being driven in a steady state between the two rollers. The two rollers press against each other (and the web), and give rise to contact pressures and shear stresses [3]. This project deals with the first case, and the various considerations that have gone into finding a theoretical solution.

A computer code NIP-SYM has been developed which can output the pressure profiles, interfacial shear stresses, deformation profiles of the rollers, as well as the velocity ratios of the web and the two rollers. The code also considers the possibility that the shear stresses between the rollers and the web could start to exceed the maximum value possible due to friction, in which case there would be slippage. This would lead to microslip over a small region of the nip for large friction coefficients, to large scale slip for small coefficients of friction. The program is written in 'C', is modular, and self contained.

CHAPTER 2

THEORETICAL BACKGROUND AND LITERATURE SURVEY

2.1 Hertz Theory - Normal Contact of Elastic Solids

The first satisfactory analysis of the stresses at the contact of two elastic solids is due to Hertz (1882) [5]. Two convex elastic bodies are initially just touching each other. The separation between the surfaces of the two bodies is initially h. Then two remote points in the bodies approach each other with respective displacements of δ_1 and δ_2. This compresses the two surfaces together over a small region of total length $2a$ called the contact width; figure 2.1. Hertzian contact can be summed up by the following two expressions. Within the zone of contact equation 2.1 is valid, whereas the inequality 2.2 holds outside of it.

$$\bar{u}_{z1} + \bar{u}_{z2} + h = \delta_1 + \delta_2 \qquad (2.1)$$

$$\bar{u}_{z1} + \bar{u}_{z2} + h > \delta_1 + \delta_2 \qquad (2.2)$$

The problem in elasticity can now be stated as follows — the distribution of mutual pressure $p(x, y)$ acting over an area S on the surface of two elastic half-spaces is required which will produce normal displacements on the surface $\bar{u}_{z1}$ and $\bar{u}_{z2}$ satisfying equation 2.1 within S and 2.2 outside it. Hertz used the following simplifying assumptions to get a solution —

1. The surfaces are continuous and nonconforming.

2. The strains are small.

3. Each solid can be considered an elastic half space.

4. The surfaces are frictionless.

For the simpler case of solids of revolution, Hertz obtained the following expression for contact pressure that satisfied both equations 2.1 and 2.2 :

$$p = p_o \{1 - (s/a)^2\}^{1/2} \qquad (2.3)$$

The nondimensionalized parabolic contact pressure profile is shown in figure 2.2. From the dis-
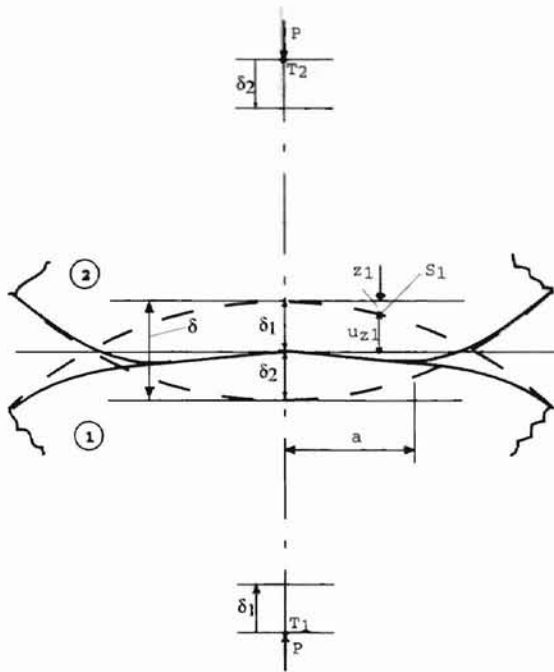
Figure 2.1: Deformation of two convex solids in contact [6].
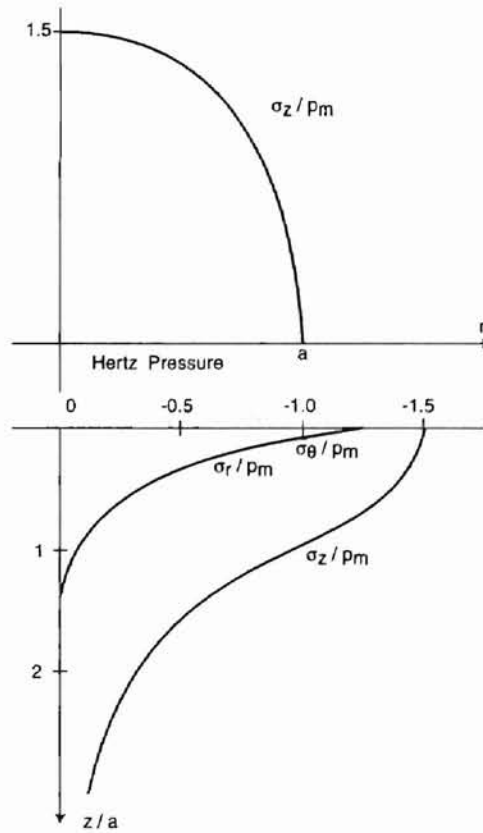
Figure 2.2: Stresses generated by Hertz contact pressure [6].
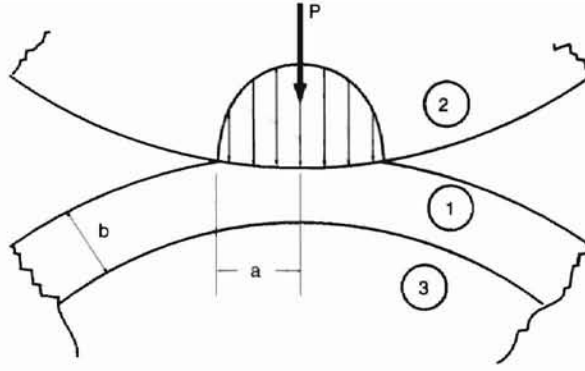
Figure 2.3: Body (2) in contact with surface layer (1) on rigid substrate (3) [6].

placement compatibility equations (equations 2.1 and 2.2) and the pressure distribution equation 2.3 one can obtain relations between the half width of contact a and p_o and between a and δ. Thus given a, the pressure distribution and deformation profile can be determined. Integration of the pressure gives the applied load.

2.2 Non-Hertzian Normal Contact of Elastic Bodies :

Here we consider the case when one or more of the Hertzian assumptions are relaxed. The contact of solids which have surface layers whose elastic properties differ from the substrate are very common; for example rubber covered rollers in processing machinery. The basic situation is illustrated in figure 2.3 where body (2) is in contact with the surface layer (1) on substrate (3). If the thickness b of the layer is large compared to the contact size $2a$, then the substrate has little influence and the contact stresses between (1) and (2) are given by the Hertz theory. For the situation where b is comparable with or less than $2a$, it has been observed that even for cases where the rollers have the same geometry and material, the limited thickness of the layer results in a relative tangential displacement at the interface which will be resisted by friction.

2.2.1 Elastic Layer on Rigid Substrate Indented by Rigid Cylinder [6]

If the contact width is small compared with the radii of curvature of the bodies, curvature of the layer can be ignored in analyzing its deformation, and the solids (2) and (3) can be taken to be elastic half spaces (figure 2.4). For a nearly incompressible layer ($\nu = 0.45 - 0.5$), the load-displacement relation is given below :

$$P = \frac{1}{3} \; \frac{(1-\nu)^2}{1-2\nu} \; \frac{E}{1-\nu^2} \; \frac{a^3}{Rb} \tag{2.4}$$

2.2.2 An Elastic Strip Between Two Elastic Rollers [6]

For a thin strip we can take the pressure distribution to be Hertzian (given by equation 2.3). A simplified solution to the integral equation for tangential traction $q(x)$ is given below:

$$q(x) = \left(1 - \frac{4\beta}{1+\alpha}\right) \; \frac{b}{2a} \; p_0 \; \frac{x}{(a^2 - x^2)^{1/2}} \tag{2.5}$$

4
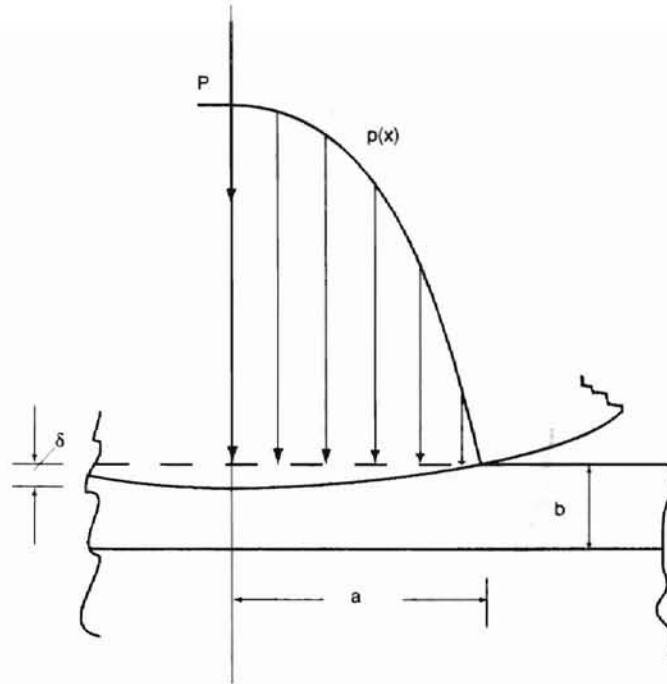
Figure 2.4: Elastic layer indented by a rigid cylinder ($\nu < 0.45$) [6].

This expression for $q(x)$ is satisfactory away from the edges of contact, but the infinite values at $x = \pm a$ are a consequence of assuming plane sections remain plane. In fact, the traction falls to zero at the edges. This is shown in figure 2.5 below:

The direction in which the tangential tractions act tend to depend on the relative elastic moduli of the strip and the rollers. Thinner strips tend to be squeezed out longitudinally and inward acting tangential tractions arise.

2.3 On Velocity Ratios - Relationship Between Local Speed and Strain

Assuming stick contact at a point inside the nip, if the common velocity of the two surfaces is $V(s)$, and the velocity at a point on the perimeter of the roller far away from the nip is V_0, the velocity ratio can be written as :

$$V(s)/V_0 = 1 + \epsilon_\theta \tag{2.6}$$

This arises because in the region of the nip, there is a circumferential strain which changes the length of the material locally. Now, the roller could be in direct contact with another roller (see Fig. 2.6) or a strip. Considering the case of a strip, a similar relation could be written for it :

$$V(s)/V_p = 1 + \epsilon_p \tag{2.7}$$

$V(s)$ is common to equations 2.6 and 2.7. Hence we obtain :

$$V_p/V_0 = \frac{1 + \epsilon_\theta}{1 + \epsilon_p} \tag{2.8}$$

5
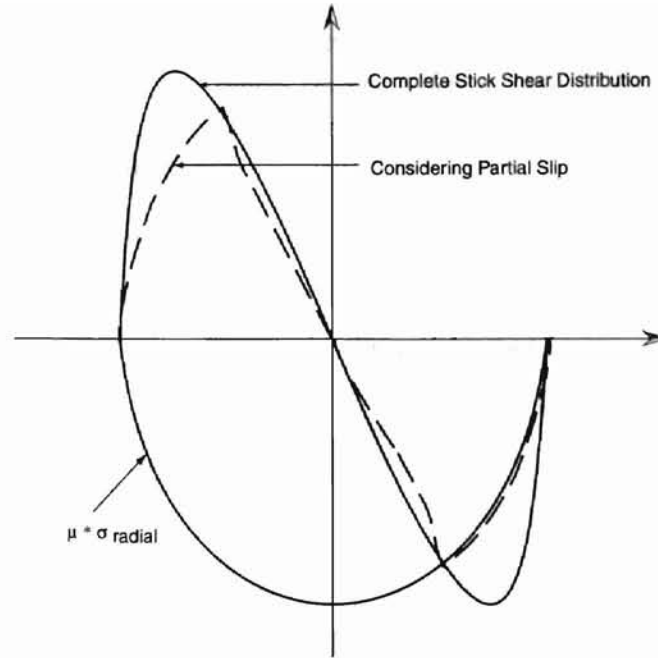
Figure 2.5: Theoretical normal $p(x)$ and shear stress $q(x)$ profiles [6].
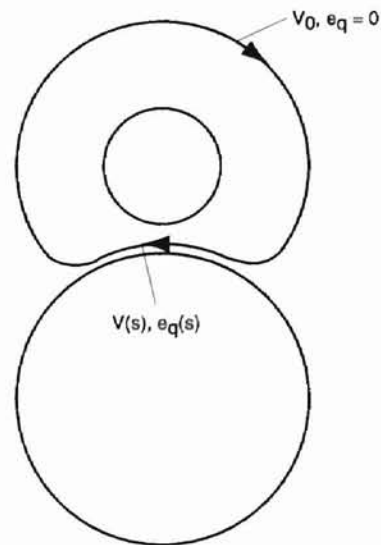
Figure 2.6: A sketch for steady state rotation [14].

6

2.4 Load Compression Relationships of Rubber Units

A couple of load-displacement relationships for rubber covered rollers are given in this section. They were used to validate the NIP-SYM code results and to compare how the code compared with Load-Deformation data obtained with rubber covered rollers at OSU WHRC.

2.4.1 The Lindley relation

The relationship given by Lindley (equation 2.9) [8] takes care of increasing rubber stiffness with deformation at the nip. The relationship is given below :

$$F = Ewt^{1/2}D^{1/2}\left(\alpha_R + \frac{kD}{t}\,\beta_R\right) \tag{2.9}$$

where

$$\alpha_R = \frac{8}{3}\ln\left(\frac{1+u^{1/2}}{1-u^{1/2}}\right) - \frac{16}{3}\,u^{1/2}$$

and

$$\beta_R = \ln\left(\frac{1+u^{1/2}}{1-u^{1/2}}\right) - \frac{10}{3}\,\frac{u^{1/2}}{(1-u)} + \frac{4u^{1/2}}{3(1-u)^2}$$

where, u is the nondimensionalized compression of rubber $= x/t$, x being the penetration and t the thickness of rubber cover. w is the width of the rubber roller cover and D is the outer diameter.

2.4.2 The Lame Relation

Using Lame's classical theory solution for the elastic stresses in a hollow cylinder subjected to external and internal pressures, the following equation can be derived [8] :

$$F = \frac{8EwD^{1/2}x^{3/2}}{3t} \tag{2.10}$$

where D is the external diameter and x the penetration. w is the width of the rubber cover and t its thickness.

2.5 Literature Survey

There are numerous investigations of contact of elastic layer-covered cylinders. Bentall and Johnson [2] studied free-rolling of dissimilar cylinders and also plane rolling contact of an elastic strip. Hahn and Levinson [4] studied a layered cylinder in contact with a hard cylinder without friction, and also for the case of gross slippage. Batra *et al.* [1] used the finite element method to study the same problem with the layer made of thermorheological material. Soong and Li [12] used the same stress function approach as used in Ref. [4] to study the contact of layered cylinders with a curled sheet in the nip. In Ref. [12], the solution was obtained by the point-matching method, instead of the Gram-Schmitd orthonormalization method used in Ref. [4].

The present study follows the method outlined by Soong and Li (Ref. [13]) for the steady rolling contact of two dissimilar cylinders, one drives the other and each cylinder is bonded with a soft layer of arbitrary thickness. There is a sheet clamped in the nip and moves with the rolling of the

Figure 2.7: Notations & Configuration of cylinders (1) and (2)

cylinders. The sheet is incompressible in its thickness, has extensional elasticity but no bending stiffness.

Local slip is accounted for at each point of contact at the interface by the criteria that shear is equal to the Coulomb friction when slip occurs, otherwise, their tangential speed at the matching point should be equal. The numerical solution is made easier by using the point-matching method (referred to from here on as the *Collocation Method*) as in Ref. [12].

Soong and Li have extended this symmetric study (Ref. [13]) to the asymmetric case (Ref. [14]) where the sheet in the nip is being pulled or pushed by a tangential force at the tail end while it is being driven in a steady state through the nip in the rollers. By increasing the tail force from zero upward, the analysis shifts from the symmetric case to the extreme case of gross slippage where the drag force is equal to or greater than the Coulomb friction between the driver and the sheet. The project started as a code for this unsymmetric case, however, there are certain complexities and ambiguities in the formulation, and it was decided that one should proceed with the symmetric case first, and gain an understanding of the equations and the collocation method. Figure 2.7 gives the notations.

2.6 Objectives and Goals

In this work, the primary objective has been to gain an understanding of the solution of nip mechanics of rollers using the collocation method developed by Soong and Li [13]. A numerical solution of the problem is sought in the form of a computer code NIP-SYM which yields the normal and shear stresses on the nip, as well as the displacements. In addition, the code is expected to generate Load-Displacement data, and the velocity ratios of the rollers and sheet. The possibility of local slippage in the nip is taken into account.

CHAPTER 3

FORMULATION OF THE PROBLEM

3.1 Stress, strain and displacements

The complete formulation can be found in the paper by Soong and Li (Ref. [12]). Here only the equations necessary to understand the NIP-SYM code are given along with explanations.

3.1.1 Stress & strain in an elastic layer bonded to a rigid core

Since both the rollers have an elastic layer bonded to a rigid core, stress, strain and displacement expressions are given for only one of them. They will be given suitable subscripts (1 for roller # 1 and 2 for roller # 2) as and when the need arises. The basic expressions for stress, strain and displacements are the same as in Ref. [4, 12, 9].

The symmetric Airy's stress function (wrt θ) for the outer soft layer of the roller can be written as :

$$U = a_0 \ln r + \frac{1}{2} b_0 r^2 + c_0 r^2 \ln r + (b_1 r^3 + c_1 r^{-1} + d_1' r \ln r) \cos \theta +$$

$$\frac{1}{2} d_1 r \theta \sin \theta + \sum_{n=2}^{\infty} (a_n r^n + b_n r^{n+2} + c_n r^{-n} + d_n r^{-n+2}) \cos(n\theta), \qquad (3.1)$$

where r and θ are coordinates. a_0, b_0 etc. are unknown constants.

The radial, tangential and shear stresses are given respectively by :

$$\sigma_r = \frac{1}{r} \frac{\partial U}{\partial r} + \frac{1}{r^2} \frac{\partial^2 U}{\partial \theta^2}, \qquad (3.2)$$

$$\sigma_\theta = \frac{\partial^2 U}{\partial r^2}, \qquad \text{and} \qquad (3.3)$$

$$\tau_{r\theta} = -\frac{\partial}{\partial r} \left(\frac{1}{r} \frac{\partial U}{\partial \theta} \right). \qquad (3.4)$$

The corresponding stress-strain relationships in terms of radial and tangential displacements u and v for an isotropic, elastic material are :

$$E\frac{\partial u}{\partial r} = \kappa\sigma_r - \beta\sigma_\theta, \tag{3.5}$$

$$E\left(\frac{u}{r} + \frac{1}{r}\frac{\partial v}{\partial\theta}\right) = \kappa\sigma_\theta - \beta\sigma_r, \qquad \text{and} \tag{3.6}$$

$$E\left(\frac{1}{r}\frac{\partial u}{\partial\theta} + \frac{\partial v}{\partial r} - \frac{v}{r}\right) = 2(1+\nu)\tau_{r\theta}. \tag{3.7}$$

where, E is the Young's modulus of the soft roll layer and κ and β are related to Poisson's ratio ν as follows : $\kappa = 1 - \nu^2, \beta = \nu(1+\nu)$, in the case of plane strain, and $\kappa = 1, \beta = \nu$, in the case of plane stress.

The nondimensionalized quantities are shown below :

$$\bar{\sigma}_r = \sigma_r/E, \quad \bar{\sigma}_\theta = \sigma_\theta/E, \quad \bar{\tau}_{r\theta} = \tau_{r\theta}/E \quad \bar{r} = r/R_0, \quad \bar{d'_1} = R_0^{-1}d'_1/E,$$

$$\bar{a}_n = R_0^{n-2}a_n/E, \quad \bar{b}_n = R_0^n b_n/E, \quad n = 0,1,2,\ldots, \tag{3.8}$$

$$\bar{c}_n = R_0^{-n-2}c_n/E, \quad \bar{d}_n = R_0^n d_n/E, \quad n = 1,2,\ldots,$$

$$\bar{u} = u/R_0, \quad \bar{v} = v/R_0.$$

From the Airy's stress function 3.1 and the equations 3.2, 3.3, 3.4 and 3.5, 3.6, 3.7 one can derive expressions for stresses, strains and displacements. One then applies the boundary conditions to determine the coefficients $\bar{a}_n, \bar{b}_n, \bar{c}_n$ and $\bar{d}_n$.

3.2 Boundary Conditions

The boundary conditions at the inner and outer radii of the hard core soft roll, with the radial and shear stress at the outer radius expressed as two Fourier series, are :

$$\bar{u} = \bar{v} = 0 \qquad\qquad \text{on } \bar{r} = \frac{r_i}{r_0} = \bar{R}_i; \tag{3.9}$$

$$\bar{\tau}_{r\theta} = \sum_{n=1}^{\infty} B_n \,\sin n\theta, \qquad \text{on } \bar{r} = 1,\ 0 \le \theta \le \pi; \tag{3.10}$$

$$\bar{\sigma}_r = \sum_{n=0}^{\infty} A_n \,\cos n\theta, \qquad \text{on } \bar{r} = 1,\ 0 \le \theta \le \pi; \tag{3.11}$$

where B_n and A_n are constants. It is to be noted that, unlike that in Ref. [4], the shear stress at the nip is, in general independent of the normal stress [13] and micro-slip may or may not occur, depending on the speed differential at each point.

Substituting the stress and displacement expressions into equations 3.9, 3.10, and 3.11 yields

$$\bar{a}_0 = \frac{(\kappa - \beta)\bar{R}_i}{(\kappa + \beta)\bar{R}_i^{-1} + (\kappa - \beta)\bar{R}_i} A_0,$$

$$\bar{b}_0 = \frac{(\kappa + \beta)\bar{R}_i^{-1}}{(\kappa + \beta)\bar{R}_i^{-1} + (\kappa - \beta)\bar{R}_i} A_0,$$

$$\bar{b}_1 = B_{12}^{-1} B_1 + B_{13}^{-1} A_1$$

$$\bar{c}_1 = B_{22}^{-1} B_1 + B_{23}^{-1} A_1 \qquad\qquad (3.12)$$

$$\bar{d}_1 = B_{32}^{-1} B_1 + B_{33}^{-1} A_1$$

$$\bar{a}_1 = -(\kappa - 3\beta)\bar{R}_i^2 \bar{b}_1 - (\kappa + \beta)\bar{R}_i^{-2}\bar{c}_1 - (\ln \bar{R}_i)\left(-\frac{(\kappa - \beta)^2}{4\kappa} + \kappa\right)\bar{d}_1$$

$$\bar{a}_n = C_{n13}^{-1} B_n + C_{n14}^{-1} A_n$$

$$\bar{b}_n = C_{n23}^{-1} B_n + C_{n24}^{-1} A_n$$

$$\bar{c}_n = C_{n33}^{-1} B_n + C_{n34}^{-1} A_n$$

$$\bar{d}_n = C_{n43}^{-1} B_n + C_{n44}^{-1} A_n$$

where $\bar{R}_i = R_i/R_0$ and B_{ij}^{-1} and C_{nij}^{-1} denote the (ij)th elements of the matrices $[B]^{-1}$ and $[C_n]^{-1}$, respectively. Matrices $[B]$ and $[C_n]$ are given below :

$$[B] = \begin{bmatrix} (6\kappa - 2\beta)\bar{R}_i^2 & 2(\kappa + \beta)\bar{R}_i^{-2} & -\beta - \frac{(\kappa - \beta)^2}{4\kappa} \\ 2 & -2 & \frac{\beta - \kappa}{4\kappa} \\ 2 & -2 & 1 + \frac{\beta - \kappa}{4\kappa} \end{bmatrix} \qquad (3.13)$$

$$[C_n] = \begin{bmatrix} C_{11} & C_{12} \\ C_{21} & C_{22} \end{bmatrix} \qquad (3.14)$$

$n = 2, 3, \ldots, \infty.$ where,

$$[C_{11}] = \begin{bmatrix} -(\kappa + \beta)n\bar{R}_i^{n-1} & -[\kappa(n - 2) + \beta(n + 2)]\bar{R}_i^{(n+1)} \\ (\kappa + \beta)n\bar{R}_i^{n-1} & [\kappa(n + 4) + \beta n)]\bar{R}_i^{(n+1)} \end{bmatrix}$$

$$[C_{12}] = \begin{bmatrix} (\kappa + \beta)n\bar{R}_i^{-(n+1)} & [\kappa(n + 2) + \beta(n - 2)]\bar{R}_i^{-(n-1)} \\ (\kappa + \beta)n\bar{R}_i^{-(n+1)} & [\kappa(n - 4) + \beta n]\bar{R}_i^{-(n-1)} \end{bmatrix}$$

$$[C_{21}] = \begin{bmatrix} n(n - 1) & n(n + 1) \\ -n(n - 1) & -(n - 2)(n + 1) \end{bmatrix}$$

$$[C_{22}] = \begin{bmatrix} -n(n + 1) & -n(n - 1) \\ -n(n + 1) & -(n + 2)(n - 1) \end{bmatrix}$$

3.3 Stress and Displacement at the Contact Arc

To separate the indented zone from the rest of the circumference which is stress-free, we assume that the radial stress and shear stress at the contact zone are expressed by Fourier series :

$$
\begin{aligned}
\bar{\sigma}_{r(\bar{r}=1)} &= \sum_{m=1}^{M} \frac{\pi}{\omega} h_m \left[(-1)^{m+1} + \cos \frac{m\pi\theta}{\omega} \right] & 0 \le \theta \le \omega \\
&= 0 & \omega \le \theta \le \pi
\end{aligned}
\tag{3.15}
$$

and

$$
\begin{aligned}
\bar{\tau}_{r\theta(\bar{r}=1)} &= \sum_{m=1}^{\bar{M}} \frac{\pi}{\omega} \tilde{h}_m \sin \frac{m\pi\theta}{\omega} & 0 \le \theta \le \omega \\
&= 0 & \omega \le \theta \le \pi
\end{aligned}
\tag{3.16}
$$

where M and $\bar{M}$ are integers. It is to be noted that at the end of the arc, $\theta = \omega$, both stresses are zero as required from contact theory.

Since the Fourier series of equations 3.10 and 3.11 cover the entire range of θ, coefficients A_n and B_n can be related to h_m and $\tilde{h}_m$ by the following equations :

$$
A_0 = \sum_{m=1}^{M} h_m (-1)^{m+1}
$$

$$
A_n = \sum_{m=1}^{M} h_m \left(\frac{\sin(m\pi - n\omega)}{m\pi - n\omega} + \frac{\sin(m\pi - n\omega)}{m\pi - n\omega} \right) \qquad n = 1, 2, \ldots, \infty
$$

$$
B_n = \sum_{m=1}^{\bar{M}} \tilde{h}_m \left(\frac{\sin(m\pi - n\omega)}{m\pi - n\omega} - \frac{\sin(m\pi - n\omega)}{m\pi - n\omega} \right) \qquad n = 1, 2, \ldots, \infty
\tag{3.17}
$$

The radial displacement, in terms of the Fourier coefficients, can be derived to yield

$$
\bar{u}(\theta) = \alpha_0 A_0 + \sum_{n=1}^{\infty} (\alpha_n A_n + \bar{\alpha}_n B_n) \cos n\theta \qquad 0 \le \theta \le \omega
\tag{3.18}
$$

where with the help of equation 3.12, the coefficients are :

$$
\alpha_0 = \frac{(\kappa^2 - \beta^2)(-\bar{R}_i + \bar{R}_i^{-1})}{(\kappa + \beta)\bar{R}_i^{-1} + (\kappa - \beta)\bar{R}_i}
$$

$$
\alpha_1 = (\kappa - 3\beta)(1 - \bar{R}_i^2) B_{13}^{-1} + (\kappa + \beta)(1 - \bar{R}_i^{-2}) B_{23}^{-1} - \left(\kappa - \frac{(\kappa - \beta)^2}{4\kappa} \right) \ln \bar{R}_i B_{33}^{-1},
$$

$$
\alpha_n = -(\kappa + \beta) n C_{n14}^{-1} - [\kappa(n-2) + \beta(n+2)] C_{n24}^{-1} + (\kappa + \beta) n C_{n34}^{-1} + [\kappa(n+2) + \beta(n-2)] C_{n44}^{-1}
\tag{3.19}
$$

$$
n = 2, 3, \ldots, \infty.
$$

$\bar{\alpha}_1$ is the same as α_1 except that the second subscript 3 in B_{i3}^{-1} is changed to 2. $\bar{\alpha}_n$ is the same as α_n except the third subscript 4 in C_{ni4}^{-1} is changed to 3.

Equation 3.18, in terms of h_m and $\bar{h}_m$, can be written as :

$$\bar{u}(\theta) = \sum_{m=1}^{M} h_m \left\{ (-1)^{m+1}\alpha_0 + \sum_{n=1}^{\infty} \alpha_n f(m,n)\cos n\theta \right\} + \sum_{m=1}^{\bar{M}} \bar{h}_m \left\{ \sum_{n=1}^{\infty} \bar{\alpha}_n \bar{f}(m,n)\cos n\theta \right\} \quad (3.20)$$

where,

$$f(m,n) = (-1)^{m+1}\frac{2\sin n\omega}{n\omega} + \frac{\sin(m\pi - n\omega)}{m\pi - n\omega} + \frac{\sin(m\pi + n\omega)}{m\pi + n\omega}$$

$$\bar{f}(m,n) = \frac{\sin(m\pi - n\omega)}{m\pi - n\omega} - \frac{\sin(m\pi + n\omega)}{m\pi + n\omega} \quad (3.21)$$

Similarly, the tangential strain at the surface can be written as

$$\epsilon_\theta(\theta) = \beta_0 A_0 + \sum_{n=1}^{\infty} (\beta_n A_n + \bar{\beta}_n B_n)\cos n\theta \qquad 0 \le \theta \le \omega \quad (3.22)$$

where

$$\beta_0 = \frac{(\kappa + \beta)(\kappa - \beta)(\bar{R}_i^{-1} - \bar{R}_i)}{(\kappa + \beta)\bar{R}_i^{-1} + (\kappa - \beta)\bar{R}_i},$$

$$\beta_1 = 2(3\kappa - \beta)B_{13}^{-1} + 2(\kappa + \beta)B_{23}^{-1} - \left(\frac{(\beta - \kappa)^2}{4\kappa} + \beta\right)B_{33}^{-1}, \quad \text{and}$$

$$\begin{aligned}
\beta_n &= n(n-1)(\kappa + \beta)C_{n14}^{-1} + (\kappa(n^2 + 3n + 2) - \beta(2 + n - n^2))C_{n24}^{-1} \\
&\quad + (\kappa + \beta)(n + n^2)C_{n34}^{-1} + (\kappa(n^2 - 3n + 2) - \beta(n^2 + n - 2))C_{n44}^{-1}
\end{aligned} \quad (3.23)$$

$\bar{\beta}_1$ is the same as β_1 except that the second subscript 3 in B_{i3}^{-1} is changed to 2. $\bar{\beta}_n$ is the same as β_n except that the third subscript 4 in C_{ni4}^{-1} is changed to 3. Similar to equation (3.20), equation 3.23 can be expressed by h_m and $\bar{h}_m$ as,

$$\epsilon_\theta(\theta) = \sum_{m=1}^{M} h_m \left\{ (-1)^{m+1}\beta_0 + \sum_{n=1}^{\infty} \beta_n f(m,n)\cos n\theta \right\} + \sum_{m=1}^{M} h_m \left\{ \sum_{n=1}^{\infty} \bar{\beta}_n \bar{f}(m,n)\cos n\theta \right\}. \quad (3.24)$$

3.4   Rolling Contact of two Cylinders

The previous equations describe the surface stress, strain and displacements for a cylinder with a soft layer in contact with other surfaces.

For the present problem, assume the other surface is also the soft layer of a cylinder. Let subscripts (1) and (2) designate the quantities related to the two cylinders, respectively.

The following two conditions, with respect to the normal pressure and indentation at the contact point, are always to be satisfied, regardless of whether there is a sheet or not :

$$(E\bar{\sigma}_r)_{(1)} = (E\bar{\sigma}_r)_{(2)} \quad (3.25)$$

$$(\bar{u}R_0)_{(1)} + (\bar{u}R_0)_{(2)} + t = u_0 + \frac{1}{2}s^2[R_{0(1)}^{-1} + R_{0(2)}^{-1}] \quad (3.26)$$

14

where t is the thickness of the sheet, u_0 is the indentation at $s = 0$, and, like the radial displacement $\bar{u}$, it is negative when displaced towards the center of the cylinder. The nip line coordinate s is defined as :

$$\theta_{(1)} = s/R_{0(1)}, \qquad \theta_{(2)} = s/R_{0(2)}. \tag{3.27}$$

Differentiation of equation 3.26 yields a relationship which is independant of u_0,

$$\frac{\mathrm{d}\bar{u}_{(1)}}{\mathrm{d}\theta} + \frac{\mathrm{d}\bar{u}_{(2)}}{\mathrm{d}\theta} = s \left[R_{0(1)}^{-1} + R_{0(2)}^{-1} \right]. \tag{3.28}$$

The other two conditions are related to shear and slip phenomena, and they are dependant on whether there is a sheet in the nip or not. In this project, it has been assumed that a sheet exists between the two rollers, so only the equations relevant to this case are given here. For the case of no sheet between rollers, see Ref. [13].

3.4.1 The Case of a Sheet in the Nip

Assume that a thin elastic sheet of infinite length is being driven by the nip of the two cylinders and there is no net force acting on the sheet. In this case, an additional unknown is introduced — the speed of the sheet outside the contact arc. Inside the nip, the steady-state speed at any point is equal to $V_p(1 + \epsilon_p(s))$ where V_p is the unknown speed outside the nip zone and ϵ_p is the local strain (see section 2.3). Since the two surfaces of the sheet are subjected to the shear stress from the two cylinders, we have,

$$\epsilon_p(s) = \frac{-1}{(tE)_p} \int_s^{L_0} \left[(E\bar{\tau}_{r\theta})_{(2)} + (E\bar{\tau}_{r\theta})_{(1)} \right] \mathrm{d}s \tag{3.29}$$

where $(tE)_p$ is the extensional stiffness of the sheet.

From equation 3.16, equation 3.29 can be written as

$$\epsilon_p(s) = \frac{1}{(tE)_p} \sum_{m=1}^{\bar{M}} ((ER_0\tilde{h}_m)_{(1)} + (ER_0\tilde{h}_m)_{(2)}) \left(\cos m\pi - \cos \frac{m\pi s}{L_0} \right) \Big/ m. \tag{3.30}$$

At a point s on cylinder (1), if the contact with the sheet is non-slip, we have

$$V_{(1)}(1 + \epsilon_{\theta(1)}) = V_p(1 + \epsilon_p) \tag{3.31}$$

which can be approximated by

$$\frac{V_p}{V_{(1)}} = 1 - \epsilon_p + \epsilon_{\theta(1)}. \tag{3.32}$$

Differentiation yields

$$\frac{\mathrm{d}\epsilon_p}{\mathrm{d}s} - \frac{\mathrm{d}}{\mathrm{d}s}\epsilon_{\theta(1)} = 0. \tag{3.33}$$

If the shear is more than what the coulomb friction can produce, we have the slip condition:

$$|\mu_{rp}E\bar{\sigma}_r|_{(1)} = |E\bar{\tau}_{r\theta}|_{(1)} \tag{3.34}$$

where μ_{rp} is the friction coefficient between the roller and the sheet.

15

Similarly, for cylinder (2), we have either

$$\frac{V_p}{V_{(2)}} = 1 - \epsilon_p + \epsilon_{\theta(2)}.$$ (3.35)

which is approximated by

$$\frac{d\epsilon_p}{ds} - \frac{d}{ds}\epsilon_{\theta(2)} = 0.$$ (3.36)

or the slipping condition,

$$|\mu_{rp}E\bar{\sigma}_r|_{(2)} = |E\bar{\tau}_{r\theta}|_{(2)}$$ (3.37)

3.5   Solution by the Collocation Method

It has been claimed by Soong and Li [12] that the point matching (collocation) method that satisfies the matching conditions at a number of discrete points on the contact arc is a much simpler technique and has an accuracy comparable to the Gram-Schmidt orthonormalization method used in Ref. [4], which solves for the coefficients h_m in series form. One of the objectives of this project has been to try and understand the intricacies of implementing this collocation method.

For the collocation method, we assume that the contact arc has a semi contact length of L_0 (symmetric about roller centerline). The contact arc is equally divided into N subdivisions. Thus, there are $N - 1$ intermediate collocation points, plus two end points at $s = 0$ and $s = L_0$.

We need to match the number of available equations with the number of unknowns. The unknowns are the coefficients h_m and $\bar{h}_m$ for both the rollers (1) and (2), the roller interference u_0, velocity ratios $\frac{V_p}{V_{(1)}}$ and $\frac{V_p}{V_{(2)}}$. However, the last three variables are differentiated out of equations 3.26, 3.32 and 3.35 to yield equations 3.28, 3.33 and 3.36. The coefficients h_m and $\bar{h}_m$ are first solved, and then they are substituted in the equations 3.26, 3.32 and 3.35 to obtain the remaining 3 unknowns u_0, $\frac{V_p}{V_{(1)}}$ and $\frac{V_p}{V_{(2)}}$.

The equations are set up as follows. For the mid point (an end point due to symmetry), one only needs to satisfy the normal stress equality equation 3.25. Also for the end point of contact there is also only one equation to be satisfied 3.28. (At these end points, the other equations effectively become of the form $0 = 0$). For the intermediate points, all the four equations 3.25, 3.28, 3.33 and 3.36 must be satisfied. This yields $4N - 2$ equations. If we choose $M = N$ and $\bar{M} = N - 1$ in equations 3.15 and 3.16, we have again $4N - 2$ number of unknown coefficients (considering both rollers). Thus the system of equations can be solved. Here, we assume that the known input parameter is the half length of nip contact L_0.

16

CHAPTER 4

ELUCIDATIONS ON THE COLLOCATION METHOD OF SOLUTION

4.1   On the Airy's Stress Function and its Solution

The stress function is derived based on purely elastic continuum mechanics principles (Ref: [9]), hence the structural behavior should be expected to be linear. This should not be taken to mean however that any load-displacement relationship is linear as well. The contact width increases with load, hence the load-displacement curve shows a stiffening effect. However, the code does not take into account any compression induced stiffening of rubber properties. This *has* been taken into account by a simplified analytical study by Lindley (see section 2.4.1).

4.2   Displacements are from an Eulerian Point of View

When we talk about displacements of the rubber in the nip region, it should be understood that this is an Eulerian displacement. That is, a material point rolls around, and hence has a velocity, but here attention is focused on a region in space. If a steady state situation is considered, a spatial point will have an unwavering value of displacement, almost like the displacement of a material point of two rollers that are pressed together statically.

4.3   Known, and to be Computed Parameters

The normal tendency is to assume that the load pressing the two rollers together is the input parameter (apart from the geometries and properties of the rollers and strip). However, in the formulation considered here, it is found that it is easier to take the semi nip length L_0 as the given quantity, from which all other parameters can be evaluated. For example, the nip load can be found by integrating the radial pressure between the rollers. Apart from the stresses, strains and

displacements, there are three main unknowns in this problem — the central overlap (interference) u_0, and velocity ratios $\frac{V_p}{V_{(1)}}$ and $\frac{V_p}{V_{(2)}}$. Any of the three quantities — the central overlap u_0, radial nip load P or the semi contact width L_0 — could have been used as the known quantity, and the other two derived from it. The semi nip length is chosen because the length along the nip s is the primary unknown in all the equations.

4.4 Relation Between the Stress Equations 3.10, 3.11 and Equations 3.15 and 3.16

The stress boundary condition requires that the normal and shear stresses be prescribed on the complete circumference of the cylinder. This is expressed as an infinite fourier series (equations 3.10 and 3.11). Stresses on the free surface are zero. The radial and normal stress on the nip are expressed as a truncated fourier series with much less number of terms (equations 3.15 and 3.16). This is possible because the nip length is very small compared to the complete circumferential length, and it needs a lot more terms of a fourier series to approximate the stress field on the circumference, than it takes to describe the parabolic profile on the nip.

The relationship between the coefficients A_n and h_m is obtained as follows :

$$\bar{\sigma}_{r(\bar{r}=1)} = \sum_{m=1}^{M} \frac{\pi}{\omega} h_m \left[(-1)^{m+1} + \cos\frac{m\pi\theta}{\omega} \right] = A_0 + \sum_{n=1}^{\infty} A_n \cos n\theta \tag{4.1}$$

For A_0 : Multiply both sides of the above equation 4.1 by $\frac{1}{\pi} \int_0^\pi \delta\hat{\theta}$.

$$A_0 = \sum_{m=1}^{M} (-1)^{m+1} h_m \tag{4.2}$$

For A_n : Multiply both sides of the above equation 4.1 by $\frac{2}{\pi} \int_0^\pi \cos k\hat{\theta}\delta\hat{\theta}$.

$$A_n = \sum_{m=1}^{M} \frac{2}{\omega} h_m (-1)^{m+1} \int_0^\omega \cos n\hat{\theta}\delta\theta + \sum_{m=1}^{M} \frac{2}{\omega} h_m \int_0^\omega \cos n\hat{\theta}.\cos\frac{m\pi\theta}{\omega}\delta\hat{\theta}$$

$$= \sum_{m=1}^{M} \frac{2}{\omega} h_m (-1)^{m+1} \frac{\sin n\omega}{n} + \sum_{m=1}^{M} h_m \left(\frac{\sin(m\pi - n\omega)}{m\pi - n\omega} + \frac{\sin(m\pi + n\omega)}{m\pi + n\omega} \right)$$

$$= \sum_{m=1}^{M} \left[(-1)^{m+1} \frac{2\sin n\omega}{n\omega} + \frac{\sin(m\pi - n\omega)}{m\pi - n\omega} + \frac{\sin(m\pi + n\omega)}{m\pi + n\omega} \right] h_m \tag{4.3}$$

The equations 4.2 and 4.3 derived above are seen to be same as equations 3.17. The relations for B_n can be derived in a similar way — multiply equation 4.1 on both sides by $\frac{2}{\pi} \int_0^\pi \cos k\hat{\theta}\delta\hat{\theta}$.

Thus, using the equations 3.21, equations 3.17 can be written as :

$$A_0 = \sum_{m=1}^{M} h_m (-1)^{m+1}$$
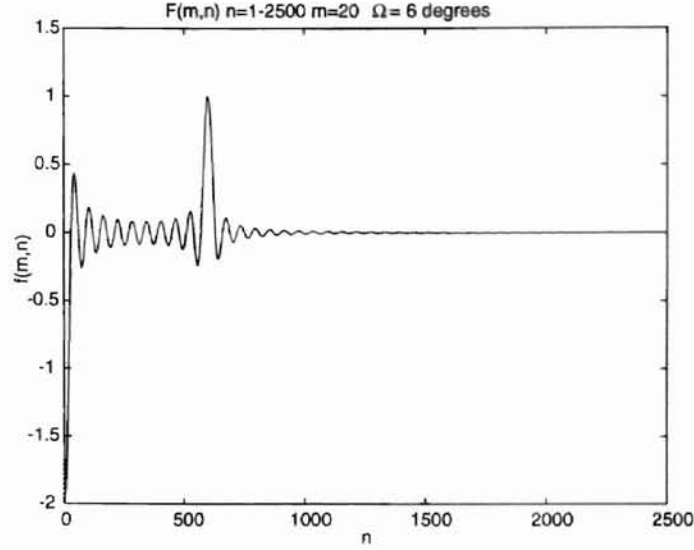
$$A_n = \sum_{m=1}^{M} h_m f(m,n) \tag{4.4}$$

18

Figure 4.1: Plot of $f(m,n)$ for $n = 1 - 2500$ and $m = 20$ ($\Omega = 6°$).

$$B_n = \sum_{m=1}^{M} \tilde{h}_m \tilde{f}(m,n)$$

4.5 On α_n, β_n and Evaluation of Strains and Displacements

α_n shows a decreasing trend with n, but never quite goes to zero. β_n on the other hand quickly saturates to a constant value. This gives rise to the possibility of certain simplifications in equation 3.24 for the evaluation of circumferential strain on the roller surface. Equation 3.24 is important for the evaluation of velocity ratios, and since the quantities of concern here are so small in magnitude, the value of circumferential strain must be properly converged.

Two approaches were adopted to obtain convergent $\epsilon_\theta(\theta)$ [10]. First, it was seen that $f(m,n)$ and $\tilde{f}(m,n)$ become negligible after around $n = 7000$. Hence the summation on n, namely, $\sum_{n=1}^{\infty}$ can be limited to $\sum_{n=1}^{7000}$ (equation 3.24). Also, since β saturates, it need not be evaluated beyond say $n = 1000$. To give an idea how the functions $f(m,n)$ and $\tilde{f}(m,n)$ behave as a function of the variable n, they are plotted below in figures 4.1 and 4.2. m has been taken as constant ($= 20$) in the figures.

Another approach is to take β out of the summation in equation 3.24. This can be done as follows :

$$\sum_{n=1}^{\infty} \beta_n f(m,n) \cos n\theta = \sum_{n=1}^{1000} (\beta_n - \beta_{1001}) f(m,n) \cos n\theta + \beta_{1001} \sum_{n=1}^{\infty} f(m,n) \cos n\theta \tag{4.5}$$

Now, the part remaining inside the summation, namely $\sum_{n=1}^{\infty} f(m,n) \cos n\theta$ can be evaluated as a closed form solution. This saves a lot of computer time. However, no closed form expression could be found for the other summation, namely, $\sum_{n=1}^{\infty} \tilde{f}(m,n) \cos n\theta$. This yields a log singularity, which cannot be integrated analytically.
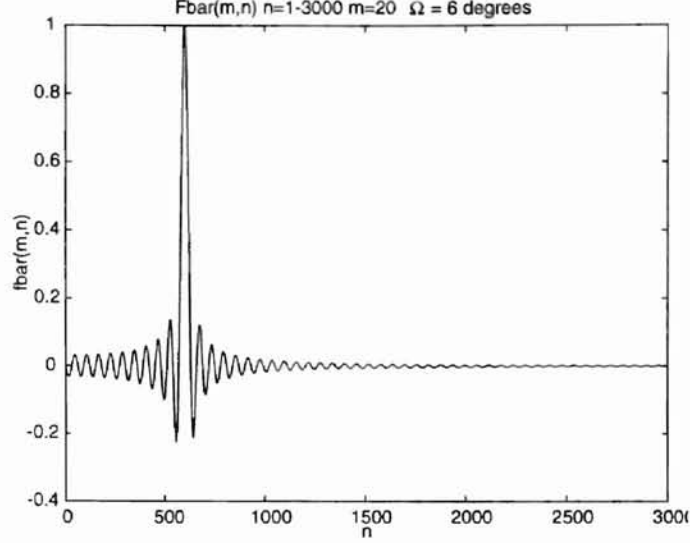
19

Figure 4.2: Plot of $\bar{f}(m,n)$ for $n = 1 - 3000$ and $m = 20$ ($\Omega = 6°$).

4.5.1 Considering the First Summation in Equation 4.5

The expression for $f(m,n)$ below has been obtained from section 4.4.

$$
\begin{aligned}
\sum_{n=1}^{\infty} f(m,n) \cos n\theta &= \frac{2}{\omega} \sum_{n=1}^{\infty} \left\{ \int_0^{\omega} \left[(-1)^{m+1} + \cos \frac{m\pi\hat{\theta}}{\omega} \right] \cos n\hat{\theta}\delta\hat{\theta} \right\} \cos n\theta \\
&= \frac{2}{\omega} \sum_{n=1}^{\infty} \left\{ \left[(-1)^{m+1} + \cos \frac{m\pi\hat{\theta}}{\omega} \right] \frac{1}{n} \sin n\hat{\theta} \Big|_0^{\omega} (\mapsto 0) \right. \\
&\quad \left. + \frac{m\pi}{\omega} \int_0^{\omega} \left[\sin \frac{m\pi\hat{\theta}}{\omega} \frac{1}{n} \sin n\hat{\theta}\delta\hat{\theta} \right] \cos n\theta \right\} \\
&= \frac{2}{\omega} \sum_{n=1}^{\infty} \left\{ \frac{m\pi}{\omega} \int_0^{\omega} \left[\sin \frac{m\pi\hat{\theta}}{\omega} \frac{1}{n} \sin n\hat{\theta}\delta\hat{\theta} \right] \cos n\theta \right\} \\
&= \frac{2m\pi}{\omega^2} \int_0^{\omega} \left\{ \sin \frac{m\pi\hat{\theta}}{\omega} \underbrace{\sum_{n=1}^{\infty} \frac{1}{n} \sin n\hat{\theta} \cos n\theta}_{F(\theta,\hat{\theta})} \right\} \delta\hat{\theta} \\
&= \frac{2m\pi}{\omega^2} \int_0^{\omega} \sin \frac{m\pi\hat{\theta}}{\omega} F(\theta,\hat{\theta})\delta\hat{\theta} \qquad (4.6)
\end{aligned}
$$

Using Mathematica, the analytical expression for $F(\theta,\hat{\theta})$ was found to be :

$$
F(\theta,\hat{\theta}) = \frac{-i}{4} \left[\ln(1 - e^{-i(\hat{\theta}-\theta)}) - \ln(1 - e^{i(\hat{\theta}-\theta)}) + \ln(1 - e^{-i(\hat{\theta}+\theta)}) - \ln(1 - e^{i(\hat{\theta}+\theta)}) \right] \qquad (4.7)
$$

In general,

$$
\ln(1 - e^{-ix}) - \ln(1 - e^{ix})
$$

20

$$= \begin{cases} -\frac{1}{4}(\pi + x) & , \quad x < 0 \\ 0 & , \quad x = 0 \\ \frac{1}{4}(\pi + x) & , \quad x > 0 \end{cases}$$

Hence $F(\theta, \hat{\theta})$ reduces to the following :

$$-\tfrac{1}{4}(\pi + \hat{\theta} - \theta) + \tfrac{1}{4}(\pi - \hat{\theta} - \theta) \quad , \quad \hat{\theta} - \theta < 0$$

$$-\tfrac{1}{4}(\pi - \hat{\theta} + \theta) + \tfrac{1}{4}(\pi - \hat{\theta} - \theta) \quad , \quad \hat{\theta} - \theta > 0$$

which simplifies to,

$$-\tfrac{\hat{\theta}}{2} \quad , \quad \hat{\theta} - \theta < 0$$

$$\tfrac{\pi}{2} - \tfrac{\hat{\theta}}{2} \quad , \quad \hat{\theta} - \theta > 0 \tag{4.8}$$

Now, the expression inside the integral of equation 4.6 can be written as :

$$-\int_0^\theta \frac{\hat{\theta}}{2} \sin \frac{m\pi\hat{\theta}}{\omega} \delta\hat{\theta} + \frac{\pi}{2} \int_\theta^\omega \sin \frac{m\pi\hat{\theta}}{\omega} \delta\hat{\theta} - \int_\theta^\omega \frac{\hat{\theta}}{2} \sin \frac{m\pi\hat{\theta}}{\omega} \delta\hat{\theta}$$

$$= \frac{\pi}{2} \int_\theta^\omega \sin \frac{m\pi\hat{\theta}}{\omega} \delta\hat{\theta} - \int_0^\omega \frac{\hat{\theta}}{2} \sin \frac{m\pi\hat{\theta}}{\omega} \delta\hat{\theta}$$

$$= -\frac{\omega}{2m} \cos m\pi + \frac{\omega}{2m} \cos \frac{m\pi\theta}{\omega} + \frac{\omega^2}{2m\pi} \cos[m\pi]$$

$$= \left[\frac{\omega^2}{2m\pi} - \frac{\omega}{2m} \right] \cos m\pi + \frac{\omega}{2m} \cos \frac{m\pi\theta}{\omega}$$

$$= \frac{\omega}{2m} \left(\frac{\omega}{\pi} - 1 \right) (-1)^m + \frac{\omega}{2m} \cos \frac{m\pi\theta}{\omega} \tag{4.9}$$

Hence the final analytical expression for $\sum_{n=1}^\infty f(m,n) \cos n\theta$ is :

$$\sum_{n=1}^\infty f(m,n) \cos n\theta = \frac{\pi}{\omega} \left(\frac{\omega}{\pi} - 1 \right) (-1)^m + \frac{\pi}{\omega} \cos \frac{m\pi\theta}{\omega} \tag{4.10}$$

4.5.2 Considering the Second Summation in Equation 4.5

A similar procedure is used to obtain an analytical expression for $\sum_{n=1}^\infty \tilde{f}(m,n) \cos n\theta$.

$$\tilde{f}(m,n) = \frac{2}{\omega} \int_0^\omega \sin \frac{m\pi\hat{\theta}}{\omega} \sin n\hat{\theta} \delta\hat{\theta}$$

$$= \frac{\sin(m\pi - n\omega)}{m\pi - n\omega} - \frac{\sin(m\pi + n\omega)}{m\pi + n\omega}$$

$$= \frac{2}{\omega} \int_0^\omega \overbrace{\sin \frac{m\pi\hat{\theta}}{\omega}}^{u} \overbrace{\sin n\hat{\theta}}^{v} \delta\hat{\theta}$$

$$= -\frac{2}{\omega} \sin \frac{m\pi\hat{\theta}}{\omega} \frac{1}{n} \cos n\theta \Big|_0^\omega \quad (\mapsto 0)$$

$$+ \frac{2m\pi}{\omega^2} \frac{1}{n} \int_0^\omega \cos \frac{m\pi\hat{\theta}}{\omega} \cos n\hat{\theta} \delta\hat{\theta} \tag{4.11}$$

21

$$\sum_{n=1}^{\infty} \tilde{f}(m,n) \cos n\theta = \frac{2m\pi}{\omega^2} \sum_{n=1}^{\infty} \frac{1}{n} \int_0^\omega \cos \frac{m\pi\hat{\theta}}{\omega} \cos n\hat{\theta} \delta\hat{\theta} \cos n\theta$$

$$= \frac{2m\pi}{\omega^2} \int_0^\omega \cos \frac{m\pi\hat{\theta}}{\omega} \underbrace{\sum_{n=1}^{\infty} \frac{1}{n} \cos n\hat{\theta} \cos n\theta}_{G(\theta,\hat{\theta})} \delta\hat{\theta}$$

$$= \frac{2m\pi}{\omega^2} \int_0^\omega \cos \frac{m\pi\hat{\theta}}{\omega} G(\theta,\hat{\theta}) \delta\hat{\theta} \qquad (4.12)$$

$G(\theta,\hat{\theta})$ is evaluated in Mathematica as follows. However, the expression thus obtained for $G(\theta,\hat{\theta})$ has a log singularity at $\theta = \hat{\theta}$ and the integral in equation 4.12 cannot be evaluated analytically (which limits its usefulness).

$$G(\theta,\hat{\theta}) = \sum_{n=1}^{\infty} \frac{1}{n} \cos n\hat{\theta} \cos n\theta$$

$$-\frac{1}{4} \left\{ \ln\left[1 - e^{i(\theta+\hat{\theta})}\right] + \ln\left[1 - e^{-i(\theta+\hat{\theta})}\right] + \ln\left[1 - e^{i(\theta-\hat{\theta})}\right] + \ln\left[1 - e^{-i(\theta-\hat{\theta})}\right] \right\}$$

Now, in general,

$$-\frac{1}{4} \left\{ \ln\left[1 - e^{ix}\right] + \ln\left[1 - e^{-ix}\right] \right\} = -\frac{1}{4} \ln\left[1 - e^{-ix} - e^{ix} + 1\right]$$

$$= -\frac{1}{4}[2 - 2\cos x]$$

Therefore,

$$G(\theta,\hat{\theta}) = -\frac{1}{4} \left\{ \ln\left[2 - 2\cos(\theta+\hat{\theta})\right] + \ln\left[2 - 2\cos(\theta-\hat{\theta})\right] \right\} \qquad (4.13)$$

To give an idea about the nature of the function $G(\theta,\hat{\theta})$, it is plotted below (figure 4.3) against the variable $\hat{\theta}$.

Hence, in equation 3.24, the first infinite summation is replaced by a finite sum and an analytical expression, whereas the second infinite summation is replaced by a finite sum and a numerical integration.

4.6 A note on slip

The way equations 3.34 and 3.37 are expressed, they are not amenable to programming. The reason is that the signs of σ_r and $\tau_{r\theta}$ are not known beforehand when the equations are being set up. One cannot take the absolute value, as σ_r and $\tau_{r\theta}$ are expressed as a sum of the coefficients h_m and $\bar{h}_m$. (Absolute value of σ_r is *not* equal to the sum of the absolute value of its coefficients).

The solution is to solve the problem in two steps. In the first step, complete stick is assumed, and the direction of shear force at each collocation point is noted. It is then a logical assumption that if
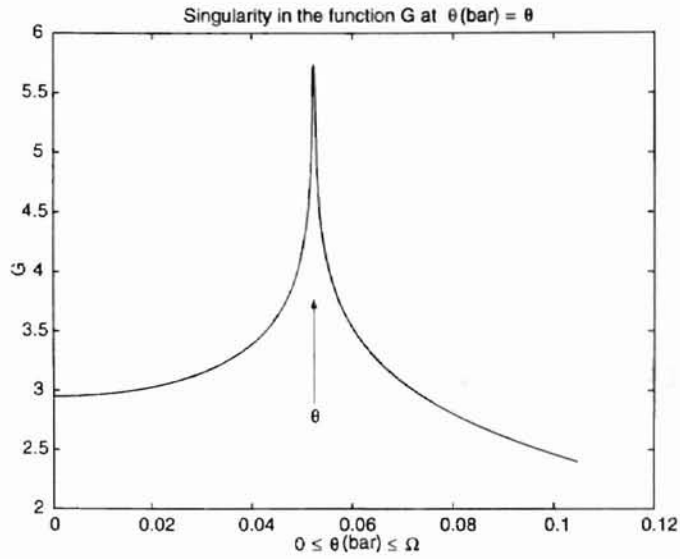
Figure 4.3: Log singularity in function $G(\theta, \hat{\theta})$.

slip occurs, the direction of shear stress at a point remains unchanged, and only the magnitude of slip gets limited by the friction law.

Initially it was felt that the slip solution had to be obtained iteratively. However, it was seen that once a collocation point is determined to be 'slip' or 'stick', its status does not change. Hence, a two step process is adequate.

It should be mentioned here that 'slip' zones and the shear stress directions ought to depend on the directions of roller surface velocity, as well as on whether the roller is the 'driver' or the 'brake'. The Soong-Li solution [13] seems to yield the solution to the static case, when two rollers are statically pressed together.

CHAPTER 5

WRITING THE NIP CODE

5.1 Introduction

The code NIP-SYM is written in 'C' and actually consists of 6 separate files. The first, nip.c, is the main program. There are 4 '.c' and 2 '.h' (header) files in all. Among the other 3 '.c' files, integ.c takes care of numerical integration and inverse.c takes care of matrix inversion. The numerical algorithms have been taken from the book 'Numerical Recipes in C' [11]. The last .c file nrutil.c consists of array handling routines from this book.

5.2 Equation Setup

It can be seen that every equation necessary in formulating the problem (3.25, 3.28, 3.33/3.34, 3.36/3.37) can be expressed in terms of the unknown coefficients h_m and $\bar{h}_m$. They are set up in the form $[K]\{h\} = \{rhs\}$. Only equation 3.28 provides a non-zero 'rhs'. The matrix equation is then solved for the coefficients h_m and $\bar{h}_m$ by inverting $[K]$.

All the routines for setting up the equations are called from the function section(). This is the heart of the nip.c program, and a study of this function should give a good idea about the way nip.c is organized. The functions for setting up the equations in turn call their own functions.

5.3 Matrix Inversion

The actual inversion of $[K]$ is carried out by the function invK(). The program was taken from 'Numerical Recipes in C' [11] and the reason it looks complex is that it requires dynamic memory allocation, and has some complicated code that makes all arrays to start with index 1 instead of 0 as is customary for the C language. The function is very accurate, and yields perfect inverses with matrices of size upto 380 x 380. The capability of the function beyond this was not checked as it was not required during the solution. It uses the LU decomposition technique.

The main matrix inversion function is stored in the inverse.c file. This file calls the auxilliary files nrutil.c, nrutil.h & nr.h. nrutil.c contains the functions for creation of dynamically allocated arrays using the malloc() memory allocation routine.

5.4   Array Storage

The routines where the displacements, strains and their derivatives are computed have a double summation, first over n, followed by a summation over m. These routines take up a lot of computer time because they call the sin() and cos() functions millions of times, and computation of sin() and cos() is expensive. Hence these terms are computed only once and stored in arrays. One drawback is that these arrays take up a huge amount of computer memory, and the code does not run on a 32 MB Pentium PC. (Upgrading the memory to 64 MB or higher should solve the problem). It needs to be executed on a mainframe computer. To eliminate this problem of large arrays, effort was made to store these arrays in direct access (or random access) files. This uses the fseek() function in C. However, accessing data from random access files turned out to take as much time (if not more) as computing the sin() and cos() functions over and over again.

5.5   The Functions main() & Restart()

The function main() calls the function section() iteratively. For a single input value of the semi nip length, it calls section() just once. For generating load-displacement data, main() calls section() iteratively for changing semi nip lengths. The user input needed to setup the solution is also coded in the function main(). User is prompted as to whether one or multiple solutions are needed. If one solution is all that is needed, next prompt asks for the semi contact angle for the first roller in degrees. If the input is for multiple angles, the user is not prompted further. Instead the program assumes that semi nip angle changes from 1 to 6 degrees, and proceeds to call section() a certain number of times. It should be mentioned here that although the user may input a round number like 6 degrees for the semi contact angle, the program adds a small fraction to it (eg. 6.000001 degrees) to avoid a potential situation where a $\sin\frac{0}{0}$ is encountered. However, this value is small, hence does not affect the final solution.

Another function called inside main() is restart(). Once a solution to the coefficients h_m and $\bar{h}_m$ are obtained, there is no need to keep reevaluating it every time an output for a new parameter is needed. The solution to the coefficients is stored in a file with a large precision, and read in when the restart() option is selected. The other option of course is a full run.

5.6   Postprocessing

In general, postprocessing is activated by uncommenting the line containing that function. It may be obtained in a full run or a restart run. It requires that certain output files be created by nip.c. This is done by setting some output file flags = 1 in the function filesopen(), which of course is called by main(). The output files have descriptive names, and a quick look should suffice to determine which output files needs to be opened for a cetain postprocessing output choice.

5.6.1 Load-Displacement Output

For the generation of load vs. displacement data, one needs to run the `nip.c` program in a loop, with a changing value of the input parameter — the semi nip length. This is controlled by the main function `main()`. The radial stress is integrated, (assuming a unit length of roller along roller axis), and the load output. In addition, the displacement of the roller is output as the central radial displacement of the collocation point lying on the centerline for roller # 1.

5.6.2 Displaced Shape

This function called `prindent()` prints out the displacements along twice the nip length. The function `indent()` does the same thing but it prints out displacements only for the collocation points, and the resulting plot could look jagged if the number of points are small. `indent()` was used primarily for checking the results when the code was being developed. `prindent()` prints the central interference, as well as the radial displacement for 200 points along twice the semi nip length, in a file `dispprint.out`. This data was then postprocessed by two small programs `circles.c` and `disp.c` to generate the displaced shapes presented in this report. `circles.c` generates the coordinates for the rigid inner cylinder, and `disp.c` generates the deformed profile of the rubber cover.

5.6.3 Stresses

Normal and shear stresses are output through the routines `printsigr()` and `printtau()`. There are corresponding routines `sigr()` and `tau()` that generated the radial stress and shear stresses on the rubber surface along the nip at the collocation points, that were primarily used for checking the code. `printsigr()` and `printtau()` printout the stresses for twice the nip length. The resulting zero stress at any coordinate outside the nip demonstrates that the boundary conditions are satisfied by the solution.

5.6.4 Velocity Ratios

The velocity ratios are obtained from equation 3.32 and 3.35. It should be remembered that the velocity ratio equations are satisfied only at the stick points, hence an attempt to evaluate them at a slip collocation point will not yield correct answers. The routines `VR1()` and `VR2()` handle the computation of velocity ratios of rollers 1 & 2. A large Young's modulus has been assumed for the strip to make the strain in the strip (ϵ_p) equal to zero. This is not necessary, but was used for validating the code, as in this case a simple inspection of the velocity ratio gives an indication of the circumferential strain. The ratios do not change over the nip length, and an evaluation at the mid point of the nip should suffice. However, the routines evaluate the ratios at all the collocation points (results at slip points will be in error).

5.6.5 Slip

As mentioned previously, slip evaluation is a two step process. First evaluation is a complete stick solution. The `slip()` function then determines which of collocation points satisfy the slip criterion,

and assign flags to them. In the next iteration these points will use the equations 3.35 and 3.37. slip() also prints out some quantities of interest, that were primarily used for checking the code. In this process, the direction of shear stress evaluated in the first iteration is important, and is used to determine the form of the slip equations.

CHAPTER 6

OBTAINING A SOLUTION

Soong and Li in their paper [13] mention that they obtained convergent solutions for $n = 450$, and that the final linear system in h_m and $\bar{h}_m$ used in equations 3.15 and 3.16 was approximately 40. The experience in developing NIP-SYM was however somewhat different. This is described in the sections below :

6.1   Oscillations

When initially attempting a complete stick solution, a high frequency oscillation in the normal stress at the nip was observed. This is quite high, of the same order as the normal stress, and cannot be ignored. This results from an abnormally high value of the coefficient h_N for both the rollers. This corresponds to the highest frequency, and the magnitude is a spurious quantity, that is, does not have any physical relevance. The correct value of the last coefficient can be obtained by solving the same problem with N augmented by 1. This introduces a new spurious last term, and the second last term is the correct last term for the previous solution. It seems to arise from the fact that there is one extra term in the equation for normal stress 3.15 ($= N$) than there is for shear stress ($= N - 1$). This was necessitated to have the number of equations equal to the number of unknowns. There also seems to be a connection between the individual components of radial and shear stress. Hence the extra ($n = N$) term for radial stress seems to be an artefact of the solution process. For the stick solution equations, the shear stresses are not directly related to the normal stresses, ie. they do not appear in the same equation, hence dropping the last term for the normal stress coefficient produces the correct normal and shear stress distributions.

For slip, the situation is more complex, as the shear stresses get directly related to the normal stresses by the slip equations, and hence incorporate the oscillations as well. This case will be discussed in the section on slip (see section 6.4.3).

6.2   Convergence

Once a reasonable normal/shear stress profile and a displaced shape at the nip is obtained, one has to check whether the results have converged. There are two variables to consider ... the number of

collocation points, and the number of terms in the infinite series in the stress equations 3.10 & 3.11. These are actually related by equations 3.17. That is because setting the number of collocation points also fixes the number of terms in the stress equations 3.15 & 3.16. One has to consider two fourier series, the first one defines the stresses over the entire perimeter (equations 3.10 & 3.11), and the other defines the same stresses but using a fourier series that has a longest period equal to the semi nip length (equations 3.15 & 3.16). Thus, one needs much fewer number of terms for the series with the smaller period. This is obvious because the smaller fourier series has to approximate a smooth continuous profile over the semi nip length, whereas the larger one approximates a discontinuous stress profile — one that is parabolic over the semi nip length and zero everywhere else on the perimeter. To ensure that both series yield the same answers, one has to take enough terms for the larger series to reproduce the highest frequency stress term of the smaller series (given by equations 3.15 & 3.16). A rough estimate can be obtained by multiplying N by the ratio of $(\pi/\text{semi nip length})$ but should be checked by using equation 3.17.

However there are situations where the theoretically required number of fourier terms in the larger series need not be adhered to. For example, during slip calculations, a large N (100 collocation points) is needed to bring down the oscillations mentioned above. However this means a very large number of terms need to be considered for the larger fourier series. But it is observed that we get reasonably converged solutions for $N = 15 \ldots 20$. Hence the extra collocation points are not really necessary, and the corresponding high frequencies can be ignored. This is specially important for small nip angles (eg. 1 degree), where the number of fourier coefficients for the larger series become inordinately high. Thus n can be limited to a reasonable value, around 3000.

It is also noticed that the shear stress takes a lot more number of terms to converge than the normal stress. However, the peak value of shear stress is not very important, as in the second iteration for slip, the shear stresses get truncated to $\mu\sigma_r$ anyway.

6.3   Code Limitations

The Soong and Li formulation [13] introduces a limitation on the maximum thickness of rubber cover given by the nondimensionalized parameter $\bar{R}_i$. Equation 3.14 has to be evaluated multiple times for increasing n. There is a problem here as the diagonal terms keep getting smaller in comparison to the other terms, with the result that beyond a certain n, the matrix cannot be inverted. For values of $\bar{R}_i$ around 1.0 (ie. a small rubber cover), the n upto which the matrix inverts correctly is high. Problem arises for lesser values of $\bar{R}_i \approx 0.85$ where the inversion problem crops up for values of n as low as 1000. This is just not enough to achieve convergence, and the error can be seen in the displacement plots (see figure 6.5).

Another limitation is that the formulation does not consider the direction of rotation of the rollers. Hence, it appears that the solution obtained really simulates the situation where two rollers are statically pressed together. The shear stresses for rollers that are in *free rolling* are not symmetric.
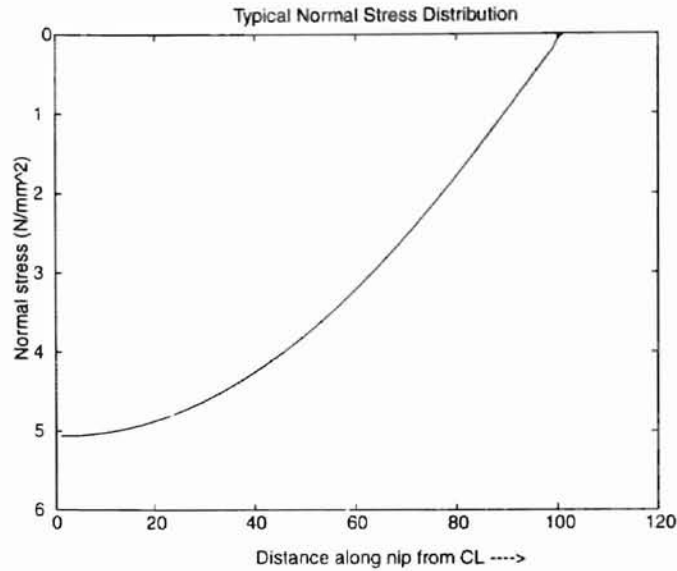
Figure 6.1: Typical normal stress profile.

6.4 Results

6.4.1 Complete Stick

Following are some plots that show the normal (Fig.6.1) and shear stress (Fig.6.2) distributions at the nip, as well as the deformation profiles for a generic problem. The first deformed shape is for the case where the rollers and rubber properties are identical (Fig.6.3). The next one is for the same problem but with a much stiffer rubber cover for one roller (Fig.6.4). The figure following this (Fig.6.5) shows the error in displacements that appear as a result of considering a larger rubber thickness ($\bar{R}_i = 0.8$).

6.4.2 Load – Displacement Curves ($P - \delta$)

To validate the stress profiles obtained earlier, $P - \delta$ curves are constructed by integrating the radial stress over the nip length, and compared with the tests on 4 different roller configurations — these tests were carried out at Oklahoma State University and 3M. For comparison, the $P - \delta$ predicted by the Lindley (2.9), Johnson (2.4) and Lame (2.10) relations are shown as well. The simplified analytical study by Lindley (see section 2.4.1) takes into account the compression induced stiffening of rubber properties. But the nip-code answers seem to match the unstiffened correlations of section 2.2.1 better. The reason probably is that in the numerical test problems that were solved with the nip-code, a maximum half contact width angle of 6° has been considered. However, this does not give sufficient rubber compression to make the stiffening effect to be felt. Also, the Lindley load-displacement expression (equation 2.9) seems to underpredict the load at small deformations. The nip code thus fares much better when compared to the 'Lame' and 'K.L. Johnson' load-displacement relations (equations 2.10 and 2.4).

The roller configurations and corresponding figure numbers are given below:
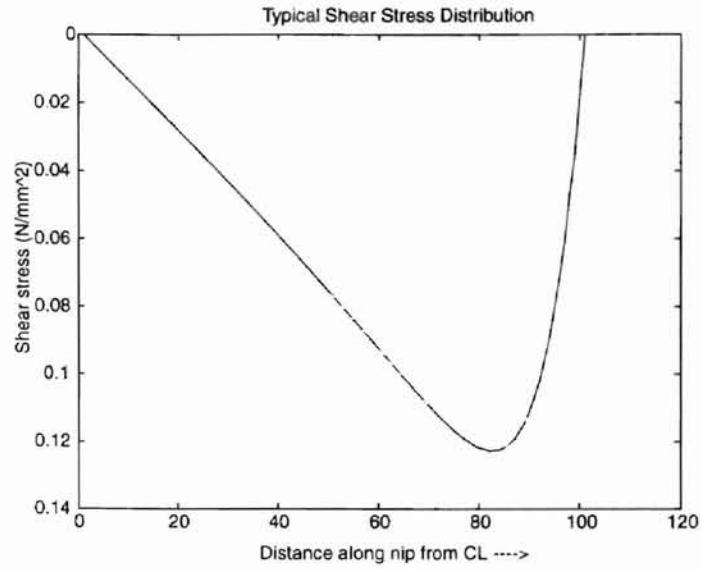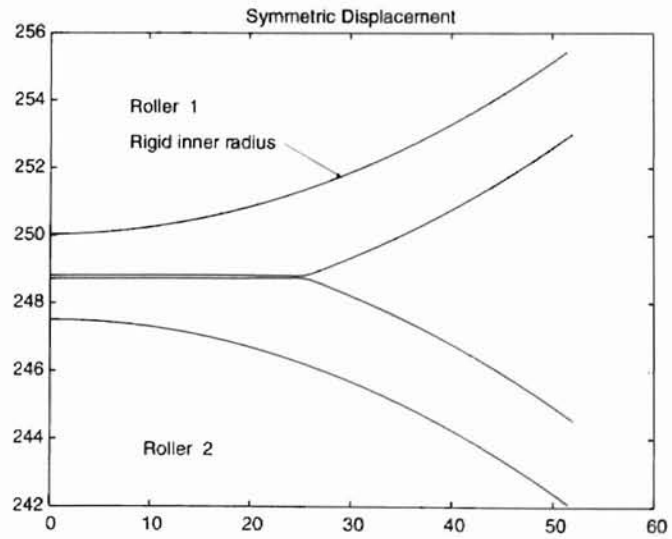
30

Figure 6.2: Typical shear stress profile.
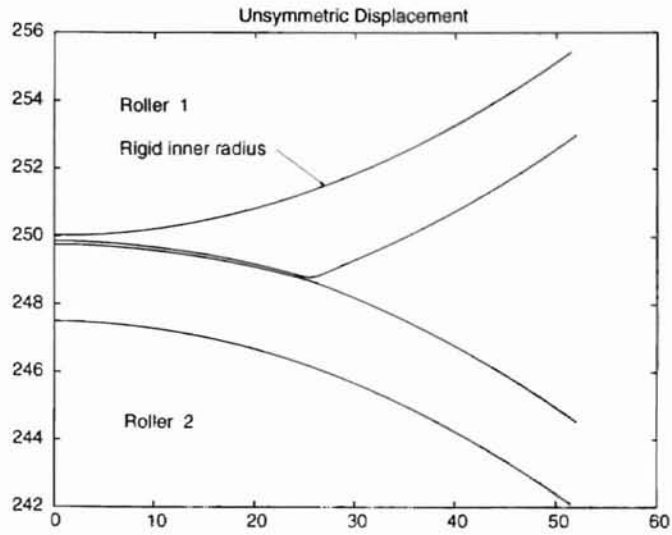

Figure 6.3: Symmetric deformed shape.

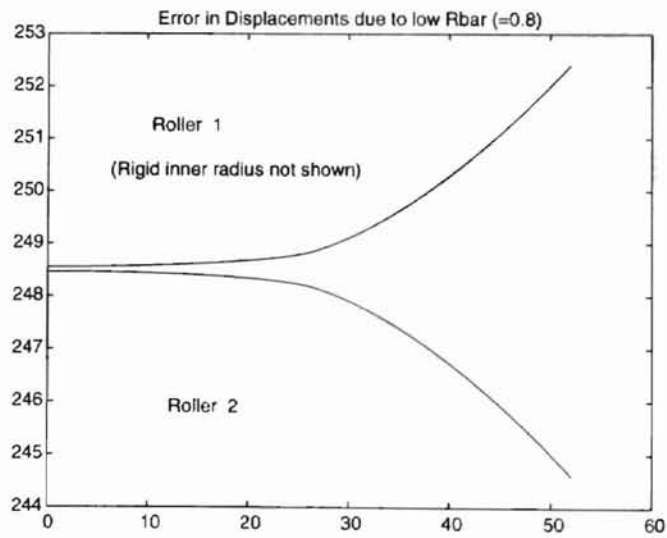Figure 6.4: Unsymmetric deformed shape — Rubber on one roller stiffer (x 10).

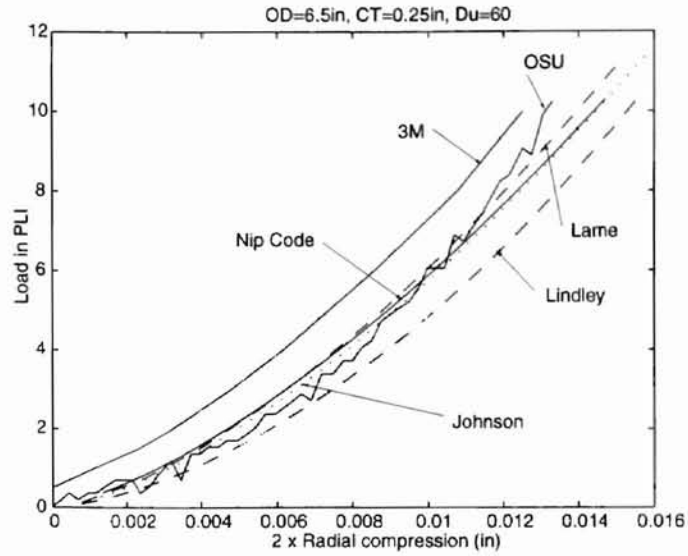Figure 6.5: Error in deformed shape : low $\bar{R}_i = 0.8$.

Figure 6.6: $P - \delta$: OD 6.5in CT 0.25in Du = 60 $\bar{R}_i = 0.92$.

Fig.6.6 :	OD 6.5in	CT 0.25in	Du = 60	$\bar{R}_i = 0.92$
Fig.6.7 :	OD 2.5in	CT 0.25in	Du = 80	$\bar{R}_i = 0.80$
Fig.6.8 :	OD 5.0in	CT 0.50in	Du = 60	$\bar{R}_i = 0.80$
Fig.6.9 :	OD 7.5in	CT 0.75in	Du = 80	$\bar{R}_i = 0.80$

where OD is the outer dia of rubber cover, CT is the cover thickness, and Du is the Young's modulus in Durometers.

A formula for convenient conversion for the Young's modulus of rubber from Durometer to 'psi' is given below :

$$E = 26.549 \exp(.0524D) \tag{6.1}$$

The table below gives the same conversion for some common Durometers :

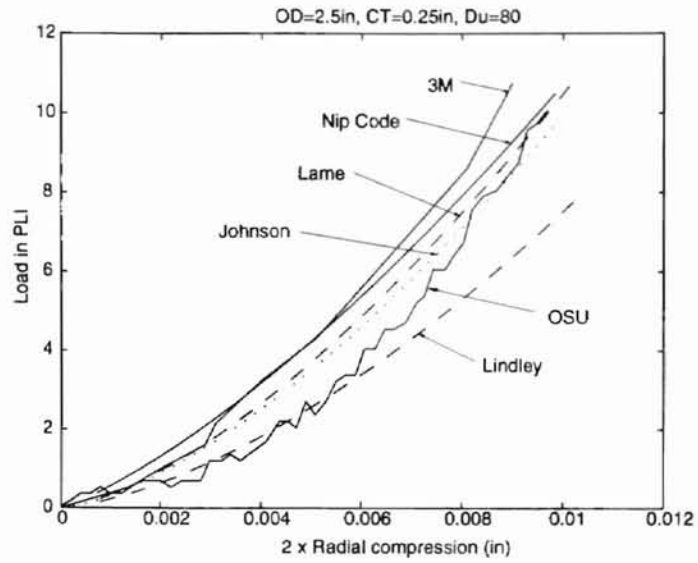| IRHD	E_0 (Young's mod-psi)
30	130
35	168
40	213
45	256
50	310
55	460
60	630
65	830
70	1040
75	1340
80	1756.4

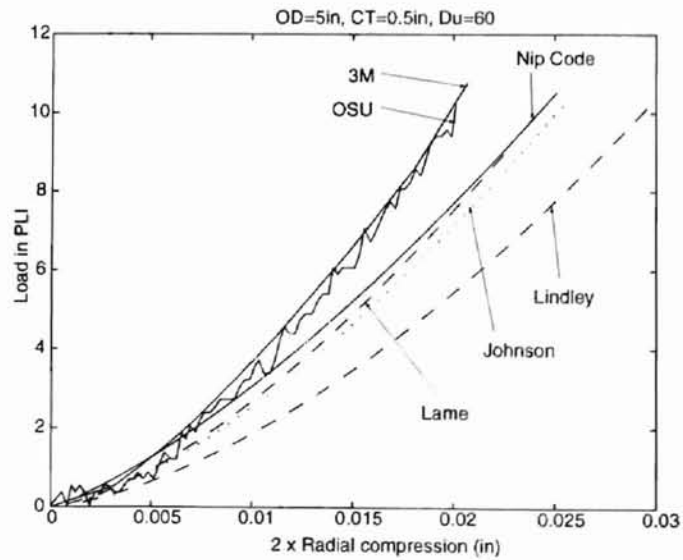Figure 6.7: $P - \delta$: OD 2.5in CT 0.25in Du = 80 $\bar{R}_i = 0.8$.

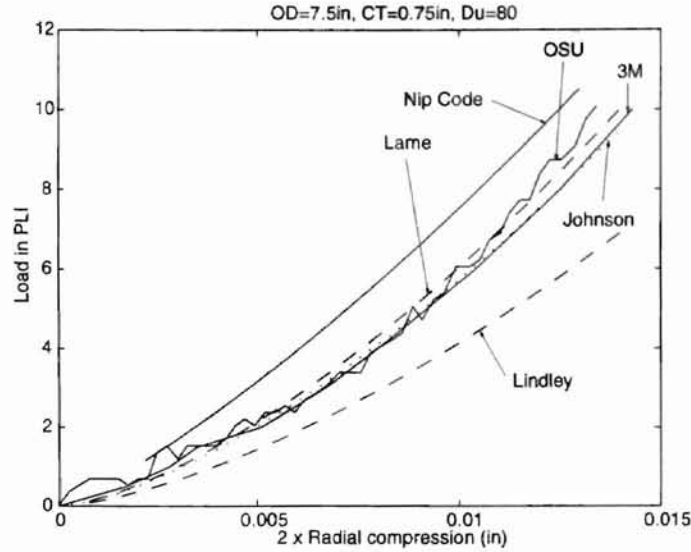Figure 6.8: $P - \delta$: OD 5.0in CT 0.5in Du = 60 $\bar{R}_i = 0.8$.

Figure 6.9: $P - \delta$: OD 7.5in CT 0.75in Du $= 80$ $\bar{R}_i = 0.8$.

6.4.3 Slip Solution

As was explained earlier, the slip solution is a two step process. First, a stick solution is obtained, and the slip locations determined. Next, for the slip zones, the slip equations are used for a second solution. It is expected that in locations where the shear stress magnitude exceeds that of the maximum possible shear allowed by friction ($|\tau| \leq \mu|\sigma_r|$), the shear stress should get limited to the value of the normal stress scaled by a factor μ, the coefficient of friction. However arriving at a slip solution required some effort, and involved making considerable changes to the coding of NIP-SYM.

For the complete stick solutions, the shear stresses are not directly connected to the normal stresses, and thus only the normal stresses showed a high frequency oscillation that could be easily got rid of by dropping the erroneous last term. However, the slip solution is a two step process, and in the second step, the shear stresses get directly related to the normal stresses in the same equation. Hence the oscillations in the normal stress make an appearance in the shear stress as well. The problem is that the oscillations are not limited to the highest frequency (shear distribution in the stick region is smooth) and just dropping the last shear term does not help. It was seen that as one increases the number of collocation points, the magnitude of the oscillation drops. At around $N = 100$ the oscillations are reasonably attenuated, and the error in the high frequency coefficients are limited to the last few terms. Thus by dropping the last 20 terms, one can obtain a good shear stress profile for slip. One should recall that one can obtain convergent solutions even with $N = 20$. So, dropping the last 20 terms out of 100 does not affect the proper solution, just eliminates the oscillation. A generic slip solution is shown in figure 6.10.

The indentation and the normal stresses are not affected by slip. Hence, if for example one has to generate $P - \delta$ curves, its not necessary to go in for a slip solution.
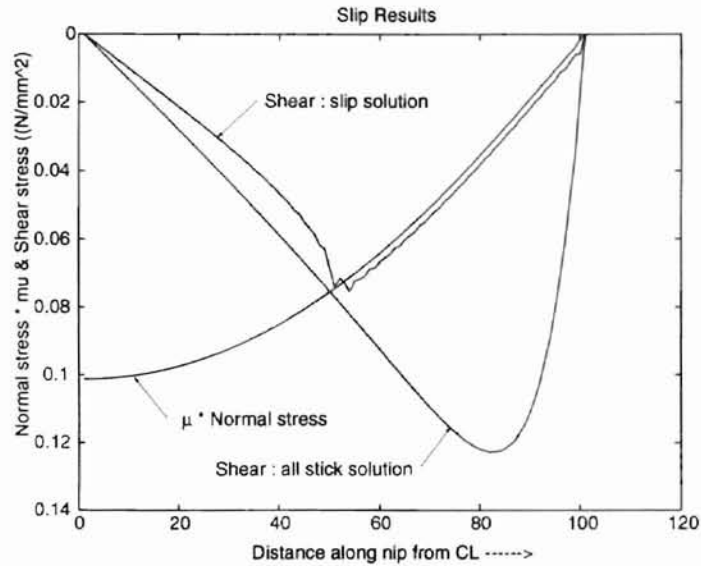
35

Figure 6.10: Slip solution : Initial and corrected shear stresses.

6.4.4 Velocity Ratios

The code outputs converged values for the velocity ratios of sheet and rollers ($\frac{V_p}{V_{(1)}}$ and $\frac{V_p}{V_{(2)}}$). The variation of velocity ratios with coefficient of friction between roller and sheet (μ_{rp}) follow the trend presented by Soong and Li [13], but the numbers are somewhat off (figure 6.11). This is essentially due to a difference in the results for circumferential strain. It can be seen from the figure that as the coefficient of friction reduces below 0.1, micro slip occurs which affects the nominal speed ratios between the sheet and the two rollers.

The variation of velocity ratio along the nip has not been plotted as it is a constant. (The ratios are between velocities outside of the nip and will remain a constant for any point within the nip).
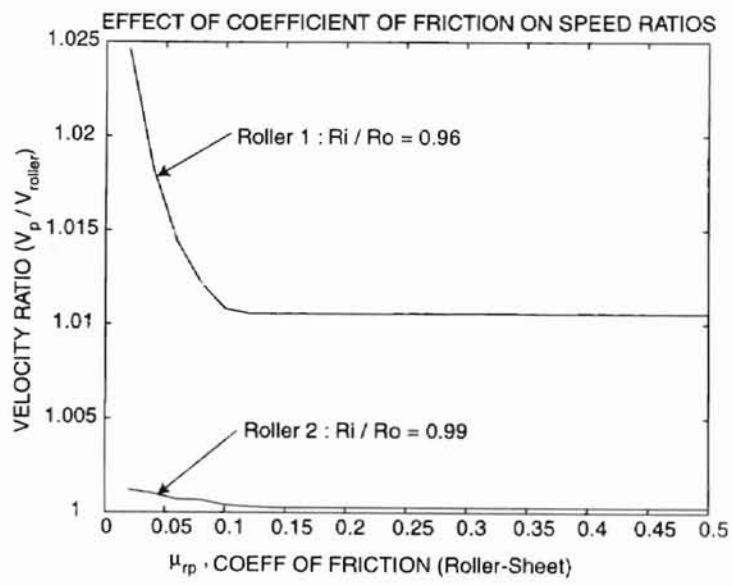
Figure 6.11: Variation of Velocity Ratios with Friction Coeff.

CHAPTER 7

CONCLUSIONS

7.1   Understanding Nip Mechanics

Considering the complexity of the subject, a reasonably good understanding of the problem has been gained during this work. The limitations and potential of the collocation method in modeling the symmetric nip mechanics of rollers has been brought out. The major limitation of the method is that it is limited to yielding correct solutions for very thin rubber covers. The solution incorporates certain oscillations that are hard to get rid of. Since convergent results are obtained with 20 collocation points, and 100 points are needed to get rid of the oscillations, the penalty in terms of computation time can be guessed. This oscillation should go away if a formulation can be found where the number of coefficients of the normal and shear stresses are equal (see equations 3.15 and 3.16). The velocity ratios have also so far not yielded the expected answers. The slip directions should depend on the rolling direction, which has not been considered in the formulation.

7.2   Goals Met

7.2.1   Load-Displacement Curves

Load-Displacement curves were obtained that match experimental data very well. This is also a very good check on the normal stresses obtained.

7.2.2   Normal and Shear Stresses

Normal stresses match the Hertzian parabolic profiles very well (equation 2.3). This is because very small indentations have been considered. Shear stresses (both with full stick and slip solutions) match the profiles given in [6].

7.2.3   Displaced Shapes

Perfect displaced shapes have been obtained when the thin rubber cover limitation has been adhered to (see figures 6.3 and 6.4).

CHAPTER 8

FUTURE WORK

The only area where the current work has fallen short is in the evaluation of the velocity ratios. Although converged solutions are obtained, they do not match the values obtained by Soong and Li [13]. The thin cover limitation can be removed by using the formulation by Jorkama [10], but it will need extensive changes to the code.

Since the problem with velocity ratios stems from an error in the evaluation of circumferential strain, a way out could be to obtain these strains using a different approach. Since rubber materials are almost incompressible, their volumetric strain should be zero. (Volumetric strain is equal to the sum of the three normal strains). As the strain along the roller axis is taken to be zero (plain strain conditions), the circumferential strain should be approximately equal to the negative of the radial strain. As the radial displacements are correct (checked against experimental load-displacement curves), presumably the radial strains are correct as well.

There are a number of other formulations that appear to be theoretically sound, and which should be explored. One such work is by Kalker [7]. Kalker uses a Green's function approach. His treatment of the rolling direction and its influence on slip seems to be more robust.

BIBLIOGRAPHY

[1] Batra, R.C., and Levinson, M., and Betz, E., 1976, *Int. J. Num. Meth. Engg*, Vol. 10, pp. 767.

[2] Bentall, R.H., and Johnson, K.L., 1968, "An Elastic Strip in Plane Rolling Contact," *International Journal of Mechanical Sciences*, Vol. 10, pp. 637–663.

[3] Good, J.K., and Wu, Z., 1993, "The Mechanism of Nip-Induced Tension in Wound Rolls," ASME JOURNAL OF APPLIED MECHANICS, Vol. 60, No. 4, pp. 942–947.

[4] Hahn, H.T., and Levinson, M., 1974, "Indentation of an Elastic Layer Bonded to a Rigid Cylinder," *International Journal of Mechanical Sciences*, Vol. 16, pp. 489–502 and 503–514.

[5] Hertz, H., 1882, "On the Contact of Elastic Solids", *J. Reine und Angewandte Mathematic*, Vol. 92, pp 156–171.

[6] Johnson, K.L., 1985, "Contact Mechanics," *Cambridge University Press*.

[7] Kalker, J.J., 1989, "Elastic and Viscoelastic Analysis of Two Multiply Layered Cylinders Rolling Over Each Other with Coulomb Friction," *TU*, Delft, Netherlands.

[8] Lindley, P.B., 1966, "Load-Compression Relationships of Rubber Units," *Journal of Strain Analysis*, Vol. 1, No. 3, pp. 190–195.

[9] Little, R.W., 1973, "Elasticity," Prentice-Hall, Englewood Cliffs, N.J., pp. 166–167.

[10] Jorkama, M, 1999, "Tractions in the rolling contact of two linear elastic orthotropic cylinders," *WHRC Report*.

[11] Numerical Recepies in C, *Cambridge University Press*.

[12] Soong, T.C., and Li, C., 1980, "On the Unbonded Contact Between Plates and Layered Cylinders," ASME JOURNAL OF APPLIED MECHANICS, Vol. 47, No. 4, pp. 841–846.

[13] Soong, T.C., and Li, C., 1981, "The Steady Rolling Contact of Two Elastic Layer Bonded Cylinders With a Sheet in the Nip," *International Journal of Mechanical Sciences*, Vol. 23, pp. 263–273.

[14] Soong, T.C., and Li, C., 1981, The Rolling Contact of Two Elastic-Layer-Covered Cylinders Driving a Loaded Sheet in the Nip," ASME JOURNAL OF APPLIED MECHANICS, Vol. 48, pp. 889–894.

VITA

Devashish Munshi

Candidate for the Degree of

Master of Science

Thesis: SYMMETRIC NIP MECHANICS

Major Field: Mechanical Engineering

Biographical:

Education: Graduated from D.A.V. Jawahar Vidya Mandir High School, Ranchi, India, in 1982; received Bachelor of Engineering degree in Mechanical Engineering from the Birla Institute of Technology, Mesra, India in July 1986. Completed the requirements for the Master of Science degree with a major in Mechanical Engineering at Oklahoma State University in May 1999.

Experience: Was Graduate Engineer for a year from July '86 to July '87 at Hindustan Motors Ltd., Calcutta, India. Subsequently, worked in the Bhabha Atomic Research Center from August '87 to July '97. Employed by the Oklahoma State University as a research assistant at the Web Handling Research Center from August '97 to May '99.